Theoretical Determinations of the Ambient Conformational Distribution and Unimolecular Decomposition of *n*-Propylperoxy Radical

John K. Merle, Carrigan J. Hayes, Sergey J. Zalyubovsky, Brent G. Glover, Terry A. Miller, and Christopher M. Hadad*

Department of Chemistry, The Ohio State University, 100 West 18th Avenue, Columbus, Ohio 43210

Received: January 25, 2005; In Final Form: February 28, 2005

The conformational distribution and unimolecular decomposition pathways for the *n*-propylperoxy radical have been generated at the CBS-QB3, B3LYP/6-31+G** and mPW1K/6-31+G** levels of theory. At each of the theoretical levels, the 298 K Boltzmann distributions and rotational profiles indicate that all five unique rotamers of the *n*-propylperoxy radical can be expected to be present in significant concentrations at thermal equilibrium. At the CBS-QB3 level, the 298 K distribution of rotamers is predicted to be 28.1, 26.4, 19.6, 14.0, and 11.9% for the gG, tG, gT, gG′, and tT conformations, respectively. The CBS-QB3 C−OO bond dissociation energy (ΔH(298 K)) for the *n*-propylperoxy radical has been calculated to be 36.1 kcal/mol. The detailed CBS-QB3 potential energy surface for the unimolecular decomposition of the *n*-propylperoxy radical indicates that important bimolecular products could be derived from two 1,4-H transfer mechanisms available at $T < 500$ K, primarily via an activated *n*-propylperoxy adduct.

I. Introduction

Peroxy radicals play an important role in the atmospheric and combustion oxidation reactions of alkanes. In the daytime troposphere, alkane oxidation is typically initiated by reaction with OH radicals to yield an alkyl radical and H_2O via C−H abstraction. Molecular oxygen can then add to the radical center of the alkyl radical, resulting in an alkylperoxy radical. Peroxy radicals are integral components in the processes leading to formation of photochemical smog. Peroxy radicals and NO, generated from combustion sources and formed in auto engine exhaust, for example, react in the lower troposphere to produce excess NO_2, which upon photolysis results in an increased ozone (O_3) concentration via the following reaction sequence:[1,2]

$$RO_2^{\bullet} + NO \rightarrow RO^{\bullet} + NO_2$$

$$NO_2 + h\nu\ (\lambda < 430\ \text{nm}) \rightarrow NO + O$$

$$O + O_2 + M \rightarrow O_3$$

In a clean troposphere, ozone would replace peroxy radicals in the above scheme resulting in no net generation of ozone.

In combustion environments, alkane oxidation is initiated by loss of a hydrogen atom, via abstraction or high-energy collisions, forming an alkyl radical that can yield an alkylperoxy radical after the addition of O_2. Low-temperature combustion environments ($T < 1000$ K)[3,4] are particularly important because mechanisms that lead to autoignition of a fuel are more prominent at these lower temperatures. The persistence of alkylperoxy radicals at lower temperatures is both pressure and temperature dependent. The pressure dependence results from the energy-rich alkylperoxy radical formed in the O_2 addition step, thereby requiring collisional stabilization to prevent return to reactants or generation of products:

$$R^{\bullet} + O_2 \rightleftharpoons RO_2^{\bullet *} + M \rightleftharpoons RO_2^{\bullet} + M^*$$

$$\Downarrow$$

Products

Thermally, alkylperoxy radicals can become unstable as temperatures approach ~600 K, for which equilibrium favors reactants, thereby resulting in a negative temperature coefficient regime. As temperatures increase further, high-temperature oxidation mechanisms predominate. At temperatures where alkylperoxy radicals are prominent, several pathways are possible. Two important pathways include self-reaction and isomerization via transfer of an alkyl hydrogen (C−H) to the terminal peroxy oxygen to form a hydroperoxyalkyl radical, typically denoted QOOH, where Q represents an alkyl group with a carbon-centered radical. Of course, by abstraction of unique primary and secondary C−H bonds, different QOOH species can be generated. Each possible QOOH species derived from a particular alkylperoxy radical can be differentiated by adding the (1,*x*n) label to Q where *x* represents the numbered displacement of the new radical center from the original radical center and n designates the type (primary, secondary) of carbon from which the hydrogen is being abstracted (Figure 1). QOOH (Figure 1) radicals may decompose unimolecularly resulting in radical propagation or react with O_2 again via addition to form a hydroperoxyalkylperoxy radical. The addition of O_2 to a QOOH is thought to be primarily responsible for chain-branching events.[5,6] Such chain-branching reactions derived from alkylperoxy radical formation under low-temperature oxidation conditions lead to autoignition which can result in engine knock in an internal combustion engine.[3]

The smallest alkylperoxy radical that can undergo an internal hydrogen transfer of significant importance in either low-temperature combustion or atmospheric processes is the ethylperoxy ($CH_3CH_2OO^{\bullet}$) radical, and it has been studied extensively both experimentally[7−14] and theoretically.[15−25] Theoretical calculations by Ignatyev et al. were important in

* Corresponding author. E-mail: hadad.1@osu.edu. Fax: (614) 292-1685.

10.1021/jp050444n CCC: $30.25
Published on Web 04/02/2005

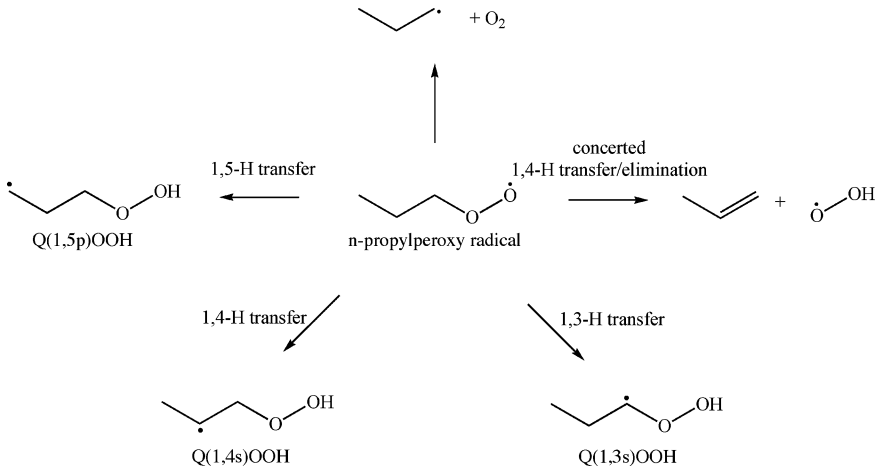

Figure 1. Potential initiation mechanisms for the unimolecular decomposition of the *n*-propylperoxy radical.

the elucidation of a 1,4-concerted elimination transition state in the ethylperoxy radical for which the abstraction of a primary hydrogen by the terminal peroxy oxygen and simultaneous cleavage of the C−O bond to form ethylene ($H_2C{=}CH_2$) and the hydroperoxy radical ($HO_2^{\bullet}$) occurs with an energetic barrier below the energy required to reform reactants, unlike that for the 1,4-transfer isomerization.[18] Prior to the study by Ignatyev et al., experimental observations had not provided conclusive evidence to rule out the direct abstraction of a primary hydrogen by O_2.

The *n*-propylperoxy ($CH_3CH_2CH_2OO^{\bullet}$) radical differs from the ethylperoxy ($CH_3CH_2OO^{\bullet}$) radical by an additional methylene ($-CH_2-$) group. The *n*-propylperoxy radical is capable of undergoing the 1,4-elimination/isomerization reactions as for the ethylperoxy radical and, additionally, due to the extra methylene group, can isomerize through a potentially low-barrier 1,5-H transfer, via a six-membered ring transition state to generate the Q(1,5p)OOH species (Figure 1).

The reaction of the propyl radical (normal and iso) with O_2 has been studied experimentally, and theoretical studies have examined several of the adduct's decomposition pathways.[5,20,26−34] Most experimental studies involve a mixture of isopropyl and *n*-propyl radicals reacting with O_2. The primary products, whether with mixed propyl radicals or an isolated *n*-propyl radical, are propene and HO_2, which seemingly can derive from 1,4-isomerization or concerted 1,4-elimination processes. Experimentally, products resulting from a 1,5-isomerization, primarily the OH radical and cyclic ethers, are negligible.[7−14] The experimental production of propene and HO_2 exhibits a pressure dependence similar to that seen in ethyl radical + O_2 studies. The pressure dependence is attributed to a mechanism by which the propene + HO_2 are derived from the chemically activated propylperoxy radical that proceeds through the low-energy barrier of the 1,4-concerted isomerization/elimination channel. Computationally, the 1,4-isomerization, concerted 1,4-elimination, and 1,5-isomerization pathways of the *n*-propylperoxy radical have been studied.[30,32,33] These studies reported that the 1,5-H transfer transition state is lower in energy than both of the 1,4-H transfer transition states and that all of these H-atom transfer barriers are calculated to be lower than the energy required for regeneration of *n*-propyl radical + O_2. DeSain et al.[30] used QCISD(T) energies for the 1,4- and 1,5-pathways to generate master equation rates to model the production of HO_2 and OH from the reactions of propyl, ethyl and butyl radicals + O_2. Niak et al.[32] used (unspecified) potential energy surfaces to study the production of HO_2 in the ethyl and propyl + O_2 systems. In each case, the 1,5-H transfer intermediate was found to be of little import.

To this point, experimental studies of the oxidation of propyl radicals by O_2 have focused on the global mechanism:

$$R^{\bullet} + O_2 \rightarrow R' + HO_2 \text{ (or OH)}$$

This paper is intended as a computational companion to an experimental study which utilized cavity ringdown spectroscopy (CRDS) for the direct detection and identification of propylperoxy radicals via the $\tilde{A}-\tilde{X}$ electronic transition.[35] The CBS-QB3 composite method as well as the B3LYP and mPW1K density functional theory (DFT) methods with the 6-31+G** basis set will be used to generate the five unique conformers of the *n*-propylperoxy radical, as well as a complete and detailed high-level potential energy surface for the unimolecular decomposition of the *n*-propylperoxy radical to yield OH, HO_2 and the closed-shell complementary species. The energetics obtained will be used to estimate the ambient distribution of each of the *n*-propylperoxy conformers and, furthermore, to predict the importance of pathways which may contribute to diminishing the abundance of detectable *n*-propylperoxy radicals, particularly those which might result from the low-energy 1,5-H transfer. We are also interested in calibrating the DFT energies and surfaces as these methods are more applicable to larger peroxy radicals.

II. Computational Methods

All calculations were performed using the Gaussian 03[36] suite of programs at the Ohio Supercomputer Center. Geometries for all stationary points were optimized using the B3LYP[37,38] and mPW1K[39] hybrid density functional theoretical methods with a 6-31+G** basis set and the composite CBS-QB3[40] method. The CBS-QB3 method attempts to estimate the CCSD(T) energy at the infinite basis set limit for a B3LYP geometry. Each stationary point was characterized via vibrational frequency calculations using the same theoretical method and basis set from which the geometry was generated. Minima were confirmed to have adequate convergence and zero imaginary vibrational frequencies. Transition state (TS) structures were confirmed to have one imaginary vibrational frequency and furthermore shown to be connected to the desired reactant and product by displacement along the normal coordinate (typically 10%) for the imaginary vibrational frequency in the positive and negative directions followed by careful minimization using either opt = calcfc or opt = calcall. For reaction coordinates

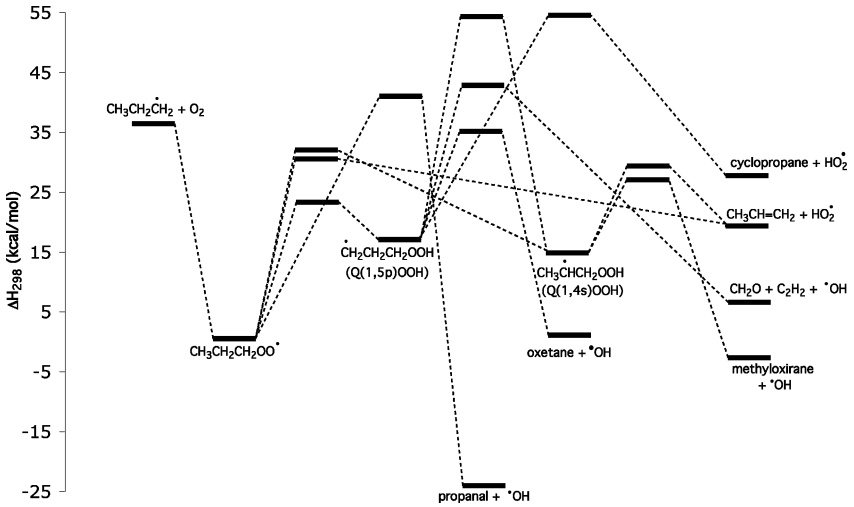

Figure 2. Potential energy diagram (ΔH_{298}, kcal/mol) at the CBS-QB3 level for the formation and unimolecular decomposition of the *n*-propylperoxy radical.

TABLE 1: CBS-QB3 Energies (CBS-QB3 and ΔH(0 K), ΔH(298 K) and ΔG(298 K) Relative to the *n*-Propylperoxy Radical) for Species Involved in Possible Unimolecular Decomposition Pathways of the *n*-Propylperoxy Radical

molecule	*E*(CBS-QB3), hartree	ΔH(0 K), kcal/mol	ΔH(298 K), kcal/mol	ΔG(298 K), kcal/mol
propyl radical (C_s) + O_2 ($^3\Sigma_g$)	−268.35291	35.1	36.5	24.3
propyl radical + O_2 ($^3\Sigma_g$)	−268.35360	34.8	36.1	24.4
O_2 ($^3\Sigma_g$)	−150.16225			
n-propylperoxy radical (gG)	−268.41016	0.0	0.0	0.0
n-propylperoxy radical (gG′)	−268.40932	0.5	0.5	0.4
n-propylperoxy radical (tG)	−268.40963	0.3	0.3	0.0
n-propylperoxy radical (gT)	−268.40972	0.2	0.3	0.2
n-propylperoxy radical (tT)	−268.40924	0.4	0.6	0.1
TS (1,5)	−268.37315	23.9	23.2	24.9
Q(1,5p)OOH[a]	−268.38409	15.9	16.4	15.6
TS (Q(1,5p)OOH → oxetane)[a]	−268.35307	35.6	35.8	35.6
oxetane + OH	−268.40995	−0.1	0.7	−7.9
TS (Q(1,5p)OOH → ethene)[a]	−268.34198	43.2	42.8	42.1
ethene + formaldehyde + OH	−268.40226	3.6	6.1	−14.7
TS (Q(1,4s)OOH → cyclopropane)[b]	−268.32325	54.2	54.5	53.6
cyclopropane + HO_2	−268.36723	26.9	27.5	17.8
TS (Q(1,5p)OOH → Q(1,4s)OOH)[a,b]	−268.32361	53.9	54.3	53.7
Q(1,4s)OOH	−268.38761	13.4	14.2	12.3
TS (Q(1,4s)OOH → methyloxirane)[b]	−268.36855	25.5	26.1	24.7
methyloxirane + OH	−268.41581	−4.0	−3.0	−12.1
TS (Q(1,4s)OOH → propene)[b]	−268.36362	28.7	29.2	28.1
propene + HO_2	−268.38036	18.2	19.3	7.6
TS ($1,4_{elim}$)[c]	−268.36102	30.9	30.8	31.2
TS (1,4)	−268.35959	32.1	31.7	32.8
TS (1,3)	−268.34509	40.9	40.8	41.0
propanal (C_s) + OH	−268.45080	−26.3	−24.9	−35.1
propanal + OH	−268.44907	−25.2	−23.8	−34.2
OH radical	−75.64736			
HO_2	−150.73824			
formaldehyde	−114.34131			

[a] Q(1,5p) designates a propyl moiety with the radical centered on the primary carbon. [b] Q(1,4s) designates a propyl moiety with the radical centered on the secondary carbon adjacent to the primary carbon. [c] "elim" distinguishes the concerted TS that includes HO_2 elimination from the formal 1,4-H transfer TS.

requiring a more accurate treatment, an intrinsic reaction coordinate (IRC)[41] calculation was performed. In general, $\langle S^2 \rangle$ values for the optimized geometries were typically $0.75 \leq \langle S^2 \rangle \leq 0.79$, except where noted in the text. The CBS-QB3 method utilizes single-point energy calculations from CCSD(T), MP4, and MP2 methods which are more susceptible to spin contamination from an unrestricted Hartree−Fock wave function. For the geometry optimization, the spin contamination is reasonable in most cases for the B3LYP optimized geometries, and the CBS-QB3 method does include a spin contamination correction term based on the deviation from the expected $\langle S^2 \rangle$ value. In the subsequent text, the Hartree−Fock $\langle S^2 \rangle$ values are not discussed but are provided in the Supporting Information.

Scaling factors of 0.9806[42] and 0.9515[43] were applied respectively to the B3LYP and mPW1K zero-point vibrational energies. Thermal corrections were determined utilizing the harmonic-oscillator/rigid-rotor approximations, using unscaled vibrational frequencies, and assuming an ideal gas at 1.0 atm. The relative weighting of each *n*-propylperoxy radical conformer was determined via a Boltzmann average as

$$N_i = \frac{g_i e^{-\Delta G_i / k_B T}}{\sum_j g_j e^{-\Delta G_j / k_B T}} \quad (1)$$

TABLE 2: B3LYP/6-31+G Energies (SCF and ΔH(0 K), ΔH(298 K) and ΔG(298 K) Relative to the *n*-Propylperoxy Radical) for Species Involved in Possible Unimolecular Decomposition Pathways of the *n*-Propylperoxy Radical**

molecule	*E* SCF, hartree	ΔH(0 K), kcal/mol	ΔH(298 K), kcal/mol	ΔG(298 K), kcal/mol
propyl radical (C_s) + O_2 ($^3\Sigma_g$)	−268.81457	30.4	31.8	19.8
propyl radical + O_2 ($^3\Sigma_g$)	−268.81493	30.1	31.4	19.8
O_2 ($^3\Sigma_g$)	−150.32758			
n-propylperoxy radical (gG)	−268.87093	0.1	0.0	0.1
n-propylperoxy radical (gG′)	−268.87019	0.5	0.5	0.5
n-propylperoxy radical (tG)	−268.87078	0.1	0.1	−0.1
n-propylperoxy radical (gT)	−268.87103	0.0	0.0	0.0
n-propylperoxy radical (tT)	−268.87082	0.0	0.1	−0.2
TS (1,5)	−268.82599	24.5	23.8	25.6
Q(1,5p)OOH[a]	−268.83770	18.7	19.3	18.0
TS (Q(1,5p)OOH → oxetane)[a]	−268.80991	35.8	35.9	35.9
oxetane + OH	−268.86141	3.0	3.8	−5.2
TS (Q(1,5p)OOH → ethene)[a]	−268.79467	43.7	44.5	42.5
ethene + formaldehyde + OH	−268.85018	4.4	6.9	−13.4
TS (Q(1,4s)OOH → cyclopropane)[b]	−268.78186	53.1	53.4	52.8
cyclopropane + HO_2	−268.82477	26.0	26.6	17.0
TS (Q(1,5p)OOH → Q(1,4s)OOH)[a,b]	−268.77566	55.3	55.6	55.2
Q(1,4s)OOH	−268.84319	15.4	16.0	14.5
TS (Q(1,4s)OOH → methyloxirane)[b]	−268.82669	24.4	25.0	23.7
methyloxirane + OH	−268.86542	−0.4	0.6	−8.5
TS (Q(1,4s)OOH → propene)[b]	−268.82423	26.6	27.0	26.0
propene + HO_2	−268.83825	16.6	17.6	6.0
TS ($1,4_{elim}$)[c]	−268.82020	27.6	27.5	27.9
TS (1,4)	−268.81247	32.8	32.4	33.5
TS (1,3)	−268.79633	42.6	42.6	42.8
propanal (C_s) + OH	−268.90232	−24.3	−22.9	−33.0
propanal + OH	−268.90103	−23.4	−22.0	−32.4
OH radical	−75.73901			
HO_2	−150.91545			
formaldehyde	−114.51152			

[a] Q(1,5p) designates a propyl moiety with the radical centered on the primary carbon. [b] Q(1,4s) designates a propyl moiety with the radical centered on the secondary carbon adjacent to the primary carbon. [c] "elim" distinguishes the concerted TS that includes HO_2 elimination from the formal 1,4-H transfer TS.

where ΔG_i is the free energy at 298 K of structure *i* relative to the structure with the lowest overall free energy set as zero, g_i is the structural degeneracy, k_B is Boltzmann's constant, *T* is temperature (298 K), and *j* runs over all five unique conformers of the *n*-propylperoxy radical. The structures, vibrational frequencies, energies, thermal corrections to the enthalpy and free energy, $\langle S^2 \rangle$ values and rotational constants for all stationary points can be found in the Supporting Information.

III. Results and Discussion

The complete CBS-QB3 potential energy surface (PES) (ΔH_{298}, kcal/mol relative to the *n*-propylperoxy radical) for the formation and unimolecular decomposition of the *n*-propylperoxy radical through 1,5-, 1,4-, and 1,3-isomerization intermediates, as well as for direct formation of propene and hydroperoxy radical via a 1,4-concerted elimination mechanism, is shown in Figure 2. Tables 1−3 list the relative enthalpies and free energies in kcal/mol relative to the *n*-propylperoxy radical for each of the stationary points at the CBS-QB3, B3LYP/6-31+G**, and mPW1K/6-31+G** levels, respectively. The discussion will focus on the energy surface as CBS-QB3 enthalpies at 298 K, unless otherwise noted.

Formation of the *n*-propylperoxy radical by the addition of O_2 ($^3\Sigma_g$) to the *n*-propyl radical is exothermic by −36.1 kcal/mol. To our knowledge, the bond dissociation energy for the C−O bond in the *n*-propylperoxy radical has not been reported. Knyazev and Slagle[44] have reported C−O bond dissociation energies for methyl, ethyl and isopropylperoxy radicals using thermochemical methods and experimental data. Table 4 shows the calculated B3LYP, mPW1K, and CBS-QB3 C−O bond dissociation energies for methyl, ethyl, isopropyl, and *n*-propylperoxy radicals vis-à-vis the experimental values. The CBS-QB3 values are in excellent agreement with the available experimental values; therefore, we expect that the calculated C−O bond dissociation energy for the *n*-propylperoxy radical is correspondingly an excellent estimate. The B3LYP and mPW1K methods appear to underestimate the BDE by ∼5 kcal/mol predicting values of −31.4 and −31.3 kcal/mol, respectively.

Five unique rotamers of the *n*-propylperoxy radical can exist in thermal equilibrium. Figure 3 shows the five possible *n*-propylperoxy radical rotamers. Each rotamer has been labeled according to the rotational orientation of the O−O−C−C (designated first) and O−C−C−C (designated second) dihedral angles in the O−O−C−C−C backbone. The two dihedral angles can have either a trans (t), a clockwise gauche (g), or a counterclockwise gauche (g′) orientation. The O−O−C−C dihedral is given a lower case notation (i.e., t or g) and the O−C−C−C dihedral an upper case notation (i.e., T or G) to differentiate each rotamer.[45] Therefore, the following unique conformations are possible: tT, tG, gG, gG′, and gT. Note that each of the conformers with a gauche orientation has an equivalent mirror image. Of significant interest are the relative stabilities of the different rotamers for the *n*-propylperoxy radical and the relative contributions of each under ambient conditions. This information will be helpful in identifying and assigning peaks in the CRDS spectrum. Table 5 provides the ΔG(298 K), percentage based on Boltzmann distribution, and degeneracy, as a result of the existence of nonsuperimposable mirror images, for each of the five unique rotamers at the CBS-QB3, B3LYP/6-31+G**, and mPW1K/6-31+G** levels. The degeneracy due to methyl rotation has been ignored because it is the same for

TABLE 3: mPW1K/6-31+G Energies (SCF and ΔH(0 K), ΔH(298 K) and ΔG(298 K) Relative to the *n*-Propylperoxy Radical) for Species Involved in Possible Unimolecular Decomposition Pathways of the *n*-Propylperoxy Radical**

molecule	*E* SCF, hartree	ΔH(0 K), kcal/mol	ΔH(298 K), kcal/mol	ΔG(298 K), kcal/mol
propyl radical (C_s) + O_2 ($^3\Sigma_g$)	−268.71796	30.4	31.8	19.6
propyl radical + O_2 ($^3\Sigma_g$)	−268.71848	30.0	31.3	19.7
O_2 ($^3\Sigma_g$)	−150.26158			
n-propylperoxy radical (gG)	−268.77457	0.0	0.0	0.1
n-propylperoxy radical (gG′)	−268.77372	0.5	0.5	0.4
n-propylperoxy radical (tG)	−268.77437	0.0	0.1	−0.1
n-propylperoxy radical (gT)	−268.77456	0.0	0.0	0.0
n-propylperoxy radical (tT)	−268.77432	0.0	0.1	−0.2
TS (1,5)	−268.72515	27.4	26.7	28.5
Q(1,5p)OOH[a]	−268.74259	18.1	18.6	17.7
TS (Q(1,5p)OOH → oxetane)[a]	−268.70362	41.8	42.1	41.4
oxetane + OH	−268.77383	−2.4	−1.6	−10.8
TS (Q(1,5p)OOH → ethene)[a]	−268.68752	51.2	51.5	50.9
ethene + formaldehyde + OH	−268.74274	11.3	13.9	−6.6
TS (Q(1,4s)OOH → cyclopropane)[b]	−268.67538	59.6	59.8	59.4
cyclopropane + HO_2	−268.72971	25.3	26.0	16.2
TS (Q(1,5p)OOH → Q(1,4s)OOH)[a,b]	−268.67672	57.2	57.4	57.2
Q(1,4s)OOH[b]	−268.74687	15.5	16.2	14.5
TS (Q(1,4s)OOH → methyloxirane)[b]	−268.72040	30.6	31.2	29.9
methyloxirane + OH	−268.77595	−4.7	−3.7	−12.8
TS (Q(1,4s)OOH → propene)[b]	−268.71619	33.8	34.2	33.2
propene + HO_2	−268.73389	21.6	22.7	10.9
TS ($1,4_{elim}$)[c]	−268.71031	36.2	37.0	36.8
TS (1,4)	−268.71098	36.1	35.7	36.8
TS (1,3)	−268.69471	46.0	45.9	46.2
propanal (C_s) + OH	−268.80766	−25.4	−24.0	−34.2
propanal + OH	−268.80612	−24.4	−23.0	−33.4
OH radical	−75.71119			
HO_2	−150.84931			
formaldehyde	−114.46153			

[a] Q(1,5p) designates a propyl moiety with the radical centered on the primary carbon. [b] Q(1,4s) designates a propyl moiety with the radical centered on the secondary carbon adjacent to the primary carbon. [c] "elim" distinguishes the concerted TS that includes HO_2 elimination from the formal 1,4-H transfer TS.

TABLE 4: Comparison of B3LYP, mPW1K, and CBS-QB3 Alkylperoxy Radical R−OO Bond Dissociation Energies (ΔH(298 K), kcal/mol) to Experimentally Derived Values

R	B3LYP[a]	mPW1K[a]	CBS-QB3	experiment[b]
methyl	−30.5	−29.8	−33.0	−32.7
ethyl	−31.4	−31.2	−35.5	−35.5
isopropyl	−31.7	−32.1	−37.6	−37.1
n-propyl	−31.4	−31.3	−36.1	N/A

[a] Geometries and energies derived from the 6-31+G** basis set. [b] See ref 44.

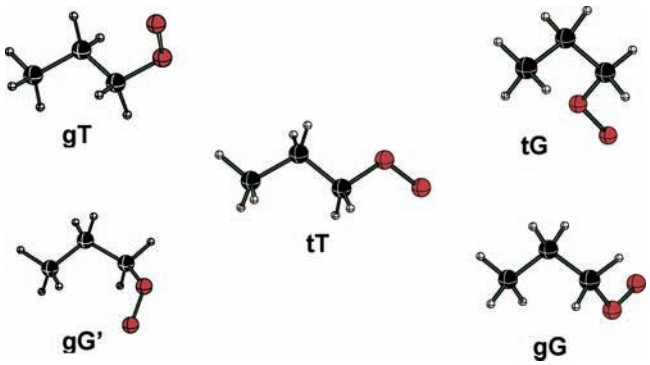

Figure 3. Five possible rotamers of the *n*-propylperoxy radical.

all rotamers. At all levels of theory, each of the five unique rotamers is consistently predicted to be present under ambient experimental conditions. At 298 K, the gG conformation is predicted to be the major contributor to the distribution, followed closely by the tG rotamer, with percentages of 28.1 and 26.4, respectively. The B3LYP and mPW1K percentages and ordering are in good agreement with each other; however, they differ from the CBS-QB3 results in this respect: favoring the tG conformation followed by the gT conformation. We have also calculated the rotational barriers (transition states) for interconversion between the different rotamers (via rotation around the C−C and C−O bonds), and the rotational barriers are all lower than 5 kcal/mol (see Supporting Information). Furthermore, at the CBS-QB3 level, the largest energy difference between the different rotamers is ΔH(298 K) = 0.6 kcal/mol. Recently, Zalyubovsky et al.[46] have proposed assignments of the observed lines in the CRDS spectrum to specific conformers. These assignments were made by comparing experimental observations to computational results, particularly for the excited $\tilde{A}$ states of both *n*-propyl peroxy and isopropyl peroxy. The intensities of the assigned lines are consistent with the predicted populations in Table 5. However the experimental results are semiquantitative at best due to partial overlap of conformer lines and unknown rotational contours.

The unimolecular decomposition of the *n*-propylperoxy radical via pathways leading to unimolecular decomposition products has been calculated and will be discussed primarily with regard to the CBS-QB3 ΔH(0 K) values, unless otherwise specifically stated. Figure 2 provides the completed potential energy surface for all of the possible unimolecular pathways accessible to the *n*-propylperoxy radical. Table 6 provides the ΔH(0 K) value for each barrier and reaction step relative to the reactant for that step at the CBS-QB3, B3LYP/6-31+G** and mPW1K/6-31+G** levels, as well as the previously calculated QCISD(T) and BH&HLYP theoretical values of DeSain et al.[30] and Chan et al.,[33] respectively. Figure 4 provides a more focused view of the initial barriers for unimolecular decomposition of

TABLE 5: Boltzmann Distributions for Each of the Five Rotamers of *n*-Propylperoxy Radical at the CBS-QB3, B3LYP/6-31+G and mPW1K/6-31+G** Levels with the Relative Free Energies (ΔG(298 K), kcal/mol) and Rotamer Degeneracy**

		CBS-QB3		B3LYP/6-31+G**		mPW1K/6-31+G**	
rotamer[a]	degeneracy[b]	ΔG(298 K)	%	ΔG(298 K)	%	ΔG(298 K)	%
gG′	2	0.41	14.0	0.62	11.8	0.57	11.7
gG	2	0.00	28.1	0.31	19.8	0.22	21.2
tG	2	0.04	26.4	0.11	27.8	0.06	28.0
gT	2	0.21	19.6	0.21	23.7	0.15	23.8
tT	1	0.10	11.9	0.00	16.8	0.00	15.4

[a] See Figure 3 for structures. [b] The degeneracy for methyl rotation has been ignored because it is the same for each rotamer.

TABLE 6: Energies, ΔH(0 K), kcal/mol, for Each Barrier and Reaction Step Relative to the Reactant for that Step at the CBS-QB3, B3LYP/6-31+G and MPW1K/6-31+G** Levels and Available Theoretical Literature Values**

molecule	ΔH(0 K) CBS-QB3	ΔH(0 K) B3LYP[a]	ΔH(0 K) mPW1K[a]	QCISD(T)[b]	BH&HLYP[c]
propyl radical + O_2 ($^3\Sigma_g$)	34.8	30.1	30.0	34.9	
n-propylperoxy radical (gG)	0.0	0.0	0.0	0.0	
TS (1,5)	23.9	24.5	27.4	23.7	30.2
Q(1,5p)OOH[d]	15.9	18.7	18.1	15.1	18.6
TS (Q(1,5p)OOH → oxetane)[d]	19.7	17.1	23.7	23.4	23.8
Oxetane + OH	−16.0	−15.7	−20.5		−20.8
TS (Q(1,5p)OOH → ethene)[d]	27.3	25.1	33.1		
ethene + formaldehyde + OH	−12.3	−14.3	−6.8		
TS (Q(1,5p)OOH → cylopropane)[d]	38.3	34.5	41.5	41.7	
cyclopropane + HO_2	11.0	7.3	7.2		
TS (Q(1,5p)OOH → Q(1,4s)OOH)[d]	38.0	36.6	39.1		
Q(1,4s)OOH	13.4	15.4	15.5	13.3	
TS (Q(1,4s)OOH → methyloxirane)[e]	12.1	9.0	15.0	15.1	
methyloxirane + OH	−17.4	−15.8	−20.2		
TS (Q(1,4s)OOH → propene)[e]	15.3	11.2	18.3		
propene + HO_2	4.8	1.1	6.0		
TS ($1,4_{elim}$)[f]	30.9	27.6	36.2	29.7	
TS (1,4)	32.1	32.8	36.1	32.3	
TS (1,3)	40.9	42.6	46.0		
propanal (C_s) + OH	−26.3	−24.3	−25.4		

[a] Geometries and energies derived form the 6-31+G** basis set. [b] Reference 30, based on basis set extrapolation scheme. [c] Reference 33, using the 6-311G** basis set. [d] Q(1,5p) designates a propyl moiety with the radical centered on the primary carbon. [e] Q(1,4s) designates a propyl moiety with the radical centered on the secondary carbon adjacent to the primary carbon. [f] "elim" distinguishes the concerted TS that includes HO_2 elimination from the formal 1,4-H transfer TS.

the *n*-propylperoxy radical with each transition state structure and ΔH(298 K) barrier height at the CBS-QB3, B3LYP/6-31+G** and mPW1K/6-31+G** levels. Moreover, Figure 5 provides a schematic view of the mechanisms studied after formation of the Q(1,5p)OOH and Q(1,4s)OOH intermediates.

The lowest barrier for isomerization of the *n*-propylperoxy radical corresponds to the 1,5-H-atom transfer that has a barrier of +23.9 kcal/mol and results in the formation of the hydroperoxypropan-3-yl radical (Q(1,5p)OOH) with a reaction endothermicity of 15.9 kcal/mol. The B3LYP barrier is in good agreement, but the mPW1K value is ∼3 kcal/mol greater. Two other theoretical barrier heights and reaction energies have been reported for the 1,5-H transfer in the *n*-propylperoxy radical. At the QCISD(T)/6-311G**+(MP2/6-311++G(2df,2pd)-MP2/6-311G**)//B3LYP/6-31G* level (hereafter just QCISD(T)), DeSain et al. calculated the ΔH(0K) activation barrier and reaction energies to be +23.7 and +15.1 kcal/mol, respectively, and at the BH&HLYP/6-311G** level, Chan et al. calculated values of +30.2 and +18.6 kcal/mol, respectively. This transition state benefits from minimal strain as a result of the six-membered ring TS. This barrier height, however, is significantly greater than those that have been estimated for the analogous 1,5-H-atom transfers in the *n*-pentyl and *n*-butoxy radicals of +17.2 and +9.2 kcal/mol, respectively, at the BAC-MP4 theoretical level.[47,48] Furthermore, this series of 1,5-H-shift reactions follows an Evans−Polanyi relationship: the *n*-butoxy, *n*-pentyl, and *n*-propylperoxy radicals, respectively, have exoergic, isoergic, and endoergic 1,5-H-transfer reactions and the barrier heights (9.2, 17.2, and 23.9 kcal/mol, respectively) follow the reaction energies accordingly.

The Q(1,5p)OOH radical can decompose by either β-scission, 1,2-H transfer isomerization, or through one of two unique cyclo-elimination processes (Figure 5). The most facile of these processes is a cyclo-elimination in which the terminal radical carbon displaces the hydroxyl radical to yield oxetane with a barrier of +19.7 kcal/mol and an exothermicity of 16.0 kcal/mol (see Figure 2). This step provides the lowest overall barrier to product formation through the Q(1,5p)OOH intermediate with an overall pathway enthalpic barrier of +35.6 kcal/mol relative to the *n*-propylperoxy radical, only 0.5 kcal/mol above the energy of the *n*-propyl radical and O_2 and slightly below their energy when considering ΔH(298 K). The B3LYP method energy deviates with a barrier ∼3 kcal/mol lower whereas the mPW1K, QCISD(T) and BH&HLYP methods all predict the barrier to be larger by ∼4 kcal/mol. The mPW1K TS wave function suffers from some spin contamination with an $\langle S^2 \rangle$ value of 0.86, rendering it somewhat suspect. The $\langle S^2 \rangle$ values for the previously reported QCISD(T) and BH&HLYP wave functions were not reported. Furthermore, the mPW1K and BH&HLYP methods predict the reaction products to be ∼4−5 kcal/mol more stable than the CBS-QB3 method. Cyclo-elimination of Q(1,5p)OOH is also possible in which cyclopropane and HO_2 are generated. The CBS-QB3 barrier height for this process is +38.3 kcal/mol with a reaction energy of +11.0 kcal/mol. The B3LYP and mPW1K barrier heights vary by ∼ −4 kcal/mol and ∼ +3 kcal/mol, respectively. The

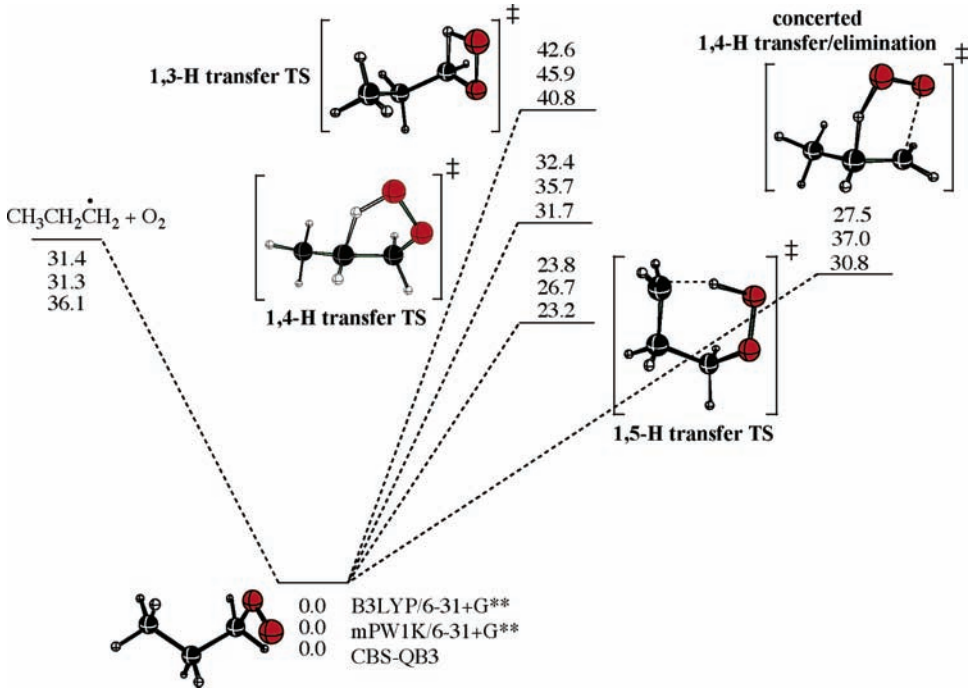

Figure 4. Energies, ΔH(298 K), kcal/mol, and typical structures for the transition states involved in the initiation of unimolecular decomposition of the *n*-propylperoxy radical. The B3LYP/6-31+G** (top), mPW1K/6-31+G** (middle), and CBS-QB3 (bottom) relative energies are provided for the respective stationary points.

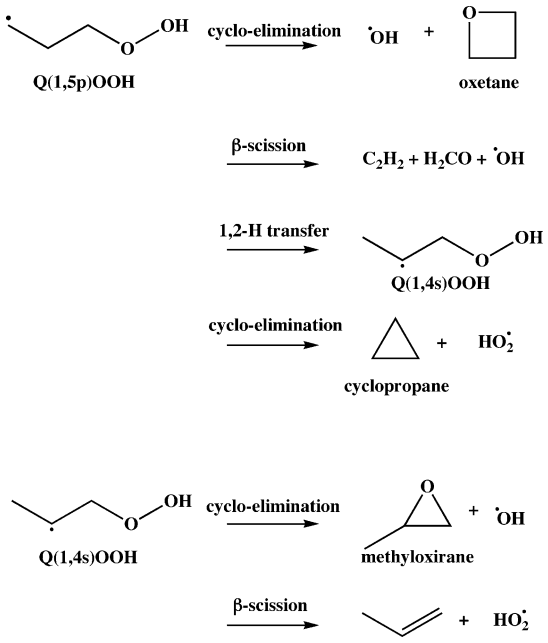

Figure 5. Schematic representation of the possible mechanisms for unimolecular decomposition for Q(1,5p)OOH and Q(1,4s)OOH.

mPW1K transition state wave function also suffers slightly from spin contamination with an $\langle S^2 \rangle$ value of 0.81. The QCISD(T) value of DeSain et al. agrees closely with the mPW1K barrier height at +41.7 kcal/mol.

Two unique transition state geometries were found for the β-scission of Q(1,5p)OOH (Figure 5). The first, and most favorable, involves coordination of the hydroperoxy hydrogen with the terminal methylene moiety, resulting in a six-membered ring transition state. The second is an extended chain structure in which no intramolecular coordination exists and is calculated to be ~1 kcal/mol higher in energy than the coordinated TS. With a calculated barrier at +27.3 kcal/mol, the β-scission of Q(1,5p)OOH yields ethane, formaldehyde, and the hydroxyl radical with an exothermicity of 12.3 kcal/mol (Figure 2). The mPW1K method once again predicts a higher energy TS, by ~6 kcal/mol, and the reaction exothermicity is smaller by ~5 kcal/mol. The β-scission route, however, requires more energy (+43.2 kcal/mol) than that gained in the formation of the *n*-propylperoxy radical and is not expected to provide a viable route for either the activated or equilibrated *n*-propylperoxy radical to proceed to products.

The 1,2-H transfer isomerization of Q(1,5p)OOH has a barrier of +38.0 kcal/mol resulting in the formation of the hydroperoxypropan-2-yl radical (Q(1,4s)OOH) with an exothermicity of 2.5 kcal/mol. The B3LYP and mPW1K barrier heights and reaction energies are in good agreement, as is the QCISD(T) reaction energy.

The Q(1,4s)OOH intermediate can undergo two relatively facile decomposition reactions. The first is a displacement of OH via cyclization that yields methyloxirane with $\Delta H^{\ddagger}(0\ \mathrm{K}) = +12.1$ kcal/mol and $\Delta H(0\ \mathrm{K}) = -17.4$ kcal/mol. The B3LYP barrier height and reaction energies are several kcal/mol below the CBS-QB3 values, whereas the mPW1K values are several kcal/mol greater. Each of the TS geometry wave functions suffers some spin contamination. The B3LYP/6-31+G** and B3LYP/CBSB7 (from the CBS-QB3 geometry optimization step) wave function have $\langle S^2 \rangle$ values of 0.80 and 0.81, respectively, and the mPW1K wave function is more suspect with a value of 0.89.[49] The QCISD(T) barrier height is in agreement with the mPW1K value at 15.1 kcal/mol. The second available reaction for the Q(1,4s)OOH intermediate is a simple β-scission resulting in propene and the hydroperoxy radical with $\Delta H^{\ddagger}(0\ \mathrm{K}) = +15.3$ kcal/mol and $\Delta H(0\ \mathrm{K}) = +4.8$ kcal/mol. The B3LYP and mPW1K energies reflect the trends seen in the step yielding methyloxirane, and the mPW1K wave function has an $\langle S^2 \rangle$ value of 0.82. Overall, reaction pathways proceeding to products through the Q(1,5p)OOH intermediate have formidable barrier heights with respect to the energetic barrier required ($\Delta H^{\ddagger}(0\ \mathrm{K}) = +8.0$ kcal/mol) to return to the *n*-propylperoxy radical. The relatively lower barrier to regenerate

TABLE 7: Thermodynamic Values, $\Delta H^{\ddagger}$ (298 K) and $\Delta G^{\ddagger}$ (298 K) kcal/mol, at the B3LYP/6-31+G Level Relative to the *n*-Propylperoxy Radical (gG) for the Transition States Involving 1,4-H Transfer Treating Internal Rotors and Frequencies as Both Harmonic and Anharmonic Oscillators**

	ΔH (298 K)			ΔG (298 K)		
	TS ($1,4_{elim}$)[a]	TS (1,4)	δTS[b]	TS ($1,4_{elim}$)[a]	TS (1,4)	δTS[b]
harm. osc.	27.1	31.9	4.88	27.5	33.1	5.54
anharm. osc.	27.4	31.7	4.31	27.8	32.6	4.88
hin. rot./harm. osc.	27.0	31.9	4.93	29.1	34.7	5.55
hin. rot./anharm. osc.	27.1	31.7	4.66	29.2	34.5	5.27

[a] "elim" distinguishes the concerted TS that includes HO_2 elimination from the formal 1,4-H transfer TS. [b] Energy difference between the two transition states [TS(1,4) − TS($1,4_{elim}$)].

the *n*-propylperoxy radical (ΔH(0 K) = +35.1 kcal/mol) makes other isomerization pathways preferable. An additional unimolecular isomerization from the Q(1,5p)OOH intermediate has been calculated by Green et al.[50] at the CBS-QB3 level in which the OH moiety is transferred to the carbon radical center. The barrier was calculated to be 27.5 kcal/mol with a considerable reaction exothermicity of 50.4 kcal/mol.

The most favorable of the two 1,4-hydrogen transfer TSs, at the CBS-QB3 level, is that of the concerted elimination in which the C−O peroxy bond breaks, whereas simultaneously abstracting a hydrogen atom on the 2-carbon of the propyl moiety with the distal end of the peroxy radical, resulting in the direct formation of propene and the hydroperoxy radical. This mechanism is analogous to the 1,4-concerted mechanism isolated in computational studies of the ethylperoxy radical.[18] The barrier for this reaction step is +30.9 kcal/mol, and the reaction is endothermic by 18.2 kcal/mol. The B3LYP values are several kcal/mol lower in energy and the mPW1K values are several kcal/mol greater than the CBS-QB3 energies. On the other hand, the previously reported QCISD(T)[30] barrier is in good agreement at $\Delta H^{\ddagger}$(0 K) = +29.7 kcal/mol. The 1,4-H transfer isomerization mechanism, resulting in the formation of Q(1,4s)OOH, has a slightly greater barrier than the concerted elimination mechanism, at 32.1 kcal/mol. Q(1,4s)OOH was shown to be derived from Q(1,5p)OOH with a barrier height ~6 kcal/mol greater that for 1,4-isomerization. Q(1,4s)OOH, furthermore, must undergo an endothermic β-scission to yield propene and the hydroperoxy radical. On the other hand, the Q(1,4s)OOH → methyloxirane + OH reaction is thermodynamically and kinetically more favorable. The B3LYP and QCISD(T) barrier heights for the 1,4-H transfer isomerization TS are in very good agreement with the CBS-QB3 values; however, the mPW1K method predicts a barrier height ~4 kcal/mol greater.

The final pathway calculated for the unimolecular decomposition of the *n*-propylperoxy radical involves a 1,3-H transfer isomerization mechanism to directly yield propanal and the hydroxyl radical. The transfer of a 1-carbon hydrogen to the terminal oxygen-centered radical simultaneously causes an OH radical to be extruded instead of a stable hydroperoxypropan-1-yl radical. The 1,3-H transfer mechanism requires a high-energy four-member ring TS with $\Delta H^{\ddagger}$(298 K) = +40.9 kcal/mol relative to the *n*-propylperoxy radical. Propanal and the hydroxyl radical are the most thermodynamically stable products obtained from the unimolecular decomposition pathways studied with an exothermicity of −25.2 kcal/mol. The B3LYP and mPW1K values are in fair agreement with only the mPW1K method predicting a barrier height 5.1 kcal/mol greater than the CBS-QB3 value. Despite the favorable reaction energy, the barrier for 1,3-H transfer is too formidable to be of significant consequence.

In summary, the most favorable kinetic process is the 1,4-H transfer that occurs concomitantly with elimination to directly generate propene and HO_2. At the CBS-QB3 level, the activation barrier is 30.8 kcal/mol (ΔH_{298}). Experimentally, Taatjes et al.[29] studied the reaction of propyl radicals with O_2 and examined the HO_2 and OH yields.[29,30] Two HO_2 source components over the 296−683 K temperature range were observed. HO_2 was found to have a minor, prompt source between 296 and 550 K, with a percent yield from 1 to 16, and a major, separate source above 550 K. The prompt production was attributed to the excited propylperoxy radical and the other, commencing at just over 500 K, to the thermalized propylperoxy radical with an activation energy for HO_2 production of 26 kcal/mol. The production of the OH radical at various temperatures was shown to have a small prompt source with a sharp increase in production above 600 K, similar to HO_2. These experimental observations are consistent with the CBS-QB3 potential energy surface that we have generated. The activated *n*-propylperoxy radical can react through the two 1,4-H transition states that lie below the energy of the *n*-propyl radical and O_2, with the concerted elimination yielding HO_2 and the isomerization yielding the OH radical. These barriers as well as the other calculated barriers, however, are too considerable to be of consequence at lower temperatures (<500 K).

To estimate potential errors in the thermodynamics associated with the harmonic-oscillator rigid-rotor approximation, the anharmonic vibrational frequencies were calculated and low-energy torsions were treated as hindered rotors to determine the corrected reaction barrier energetics for both the 1,4-H transfer and concerted 1,4-H transfer/elimination reactions at the B3LYP/6-31+G** level. These two transition states provide the most competitive decomposition pathways to generate bimolecular products. The reduced moment of inertia is calculated about the axis which includes the twisting bond. Each hindered rotor's contribution to the thermodynamic parameters was determined by generating a rigid potential energy profile of each internal rotor. The profiles were used to generate a hindrance potential as a Fourier series to construct the Hamiltonian. Using the free internal rotation wave functions as a basis, the hindered rotor energy levels were calculated by direct diagonalization of the Hamiltonian matrix. The hindered rotor partition functions were obtained via summation over the energy levels.[51] Table 7 contains the 298 K enthalpic and free energy barriers for the two 1,4-H transfer reactions determined using the harmonic-oscillator rigid-rotor approximation, anharmonic-oscillator, hindered rotor, and a combination of hindered-rotor anharmonic oscillator treatments. The change in enthalpic barrier due to the refined treatments is very small, +0.3 kcal/mol between the harmonic and anharmonic oscillator treatments for the concerted 1,4-H transfer/elimination barriers. The anharmonic treatment yielded no significant change in the free energy barriers as well. Treatment of internal rotors as hindered rotors, on the other hand, increased the free energy barriers by ~1.5 kcal/mol. This increase is attributed to a substantial gain in entropy for the *n*-propylperoxy radical due to its three internal rotors versus one for each of the transition states.

IV. Conclusions

The conformational distribution and unimolecular decomposition pathways for the *n*-propylperoxy radical have been generated by high-level theoretical methods. At room temperature, each of the five unique rotamers of the *n*-propylperoxy radical can be expected to be present and contribute to the CRDS spectrum. At the CBS-QB3 level, the 298 K distribution of rotamers is predicted to be 28.1, 26.4, 19.6, 14.0, and 11.9% for the gG, tG, gT, gG′, and tT conformations, respectively. The B3LYP and mPW1K distributions vary with respect to the most favorable rotamers. There is a significant deviation between the CBS-QB3 and two hybrid DFT methods, on the order of ∼4−5 kcal/mol, in calculating the C−OO bond energy. This points to a systematic problem for hybrid DFT methods causing these bond energies to be underestimated. Aside from underestimating the C−OO bond energy, the B3LYP/6-31+G** transition state and reaction energies are in very good agreement with the CBS-QB3 values, suggesting promising utility for studying unimolecular potential energy surfaces of larger alkylperoxy radical systems. The mPW1K/6-31+G** method, on the other hand, provided transition state energies which were significantly larger than the CBS-QB3 values.

The $C-O_2$ bond dissociation energy in the *n*-propylperoxy radical is predicted at the CBS-QB3 level to be 36.1 kcal/mol. *n*-Propylperoxy radicals are stable, at temperatures commensurate with those in the troposphere, to unimolecular decomposition as a result of formidable barriers (∼30 kcal/mol) to formation of bimolecular products. There appears to be a much greater propensity for bimolecular product formation to dominate reactivity in oxidizing environments at temperatures above 500 K. The lowest barrier height to produce bimolecular products, from the *n*-propylperoxy radical, occurs through the concerted 1,4-H-atom transfer and elimination transition state which has a $\Delta H^{\ddagger}(0\ \mathrm{K}) = +30.9$ kcal/mol, relative to the *n*-propylperoxy radical and leads directly to propene and the HO_2 radical. Furthermore, despite a lower TS energy for the 1,5-isomerization ($\Delta H^{\ddagger}(0\ \mathrm{K}) = +23.9$ kcal/mol, relative to the *n*-propylperoxy radical), the subsequent steps for Q(1,5p)OOH decomposition must proceed through significantly higher energetic barriers, thereby rendering its unimolecular decomposition products unlikely.

Acknowledgment. We gratefully acknowledge The Ohio State University Environmental Molecular Science Institute (EMSI, CHE-0089147), funded by NSF, National Science Foundation Grant No. 0211281, and the Ohio Supercomputer Center. Financial support from GAANN fellowships (J.K.M., C.J.H.) and an Amoco fellowship (J.K.M.) are gratefully appreciated. We also thank Dr. Timothy Barckholtz for providing software to perform the hindered rotor analysis.

Supporting Information Available: Energies, enthalpies, free energies as a function of temperature, and moments of inertia for all intermediates and transition states. Cartesian coordinates and harmonic vibrational frequencies for all intermediates and transition states. Rotational profiles. This material is available free of charge via the Internet at http://pubs.acs.org.

References and Notes

(1) Finlayson-Pitts, B. J.; Pitts, J. N., Jr. *Chemistry of the Upper and Lower Atmosphere: Theory, Experiments, and Applications*; Academic Press: San Diego, CA, 2000.

(2) Wallington, T. J.; Dagaut, P.; Kurylo, M. *Chem. Rev.* **1992**, *92*, 667−710.

(3) Compton, R. G.; Hancock, G. *Comprehensive Chemical Kinetics, Low-Temperature Combustion and Autoignition*; Pilling, M. J., Ed.; Elsevier: Amsterdam, 1997; Vol. 35.

(4) Glassman, I. *Combustion*; Academic Press: San Diego, CA, 1996.

(5) Bozzelli, J. W.; Pitz, W. J. *Twenty-Fifth Symposium (International) on Combustion*; The Combustion Institute: Pittsburgh, PA, 1994; pp 783−791.

(6) Bozzelli, J. W.; Sheng, C. *J. Phys. Chem. A* **2002**, *106*, 1113−1121.

(7) Wagner, A. F.; Slagle, I. R.; Sarzynski, D.; Gutman, D. *J. Phys. Chem.* **1990**, *94*, 1853.

(8) Kaiser, E. W.; Wallington, T. J.; Andino, J. M. *Chem. Phys. Lett.* **1990**, *168*, 309.

(9) Kaiser, E. W.; Rimai, L.; Wallington, T. J. *J. Phys. Chem.* **1989**, *93*, 4094.

(10) Kaiser, E. W.; Lorkovic, I. M.; Wallington, T. J. *J. Phys. Chem.* **1990**, *94*, 3352.

(11) Dobis, O.; Benson, S. W. *J. Am. Chem. Soc*. **1993**, *115*, 8798.

(12) Kaiser, E. W. *J. Phys. Chem. A* **2002**, *106*, 1256.

(13) Kaiser, E. W. *J. Phys. Chem.* **1995**, *99*, 707.

(14) Clifford, E. P.; Farrell, J. T.; DeSain, J. D.; Taatjes, C. A. *J. Phys. Chem. A* **2000**, *104*, 11549.

(15) Bozzelli, J. W.; Dean, A. M. *J. Phys. Chem.* **1990**, *94*, 3313.

(16) Quelch, G. E.; Gallo, M. M.; Schaefer, H. F., III. *J. Am. Chem. Soc.* **1992**, *114*, 8239.

(17) Quelch, G. E.; Gallo, M. M.; Shen, M.; Xie, Y.; Schaefer, H. F., III.; Moncrief, D. *J. Am. Chem. Soc.* **1994**, *116*, 4953.

(18) Ignatyev, I. S.; Xie, Y.; Allen, W. D.; Schaefer, H. F., III. *J. Chem. Phys.* **1997**, *107*, 141.

(19) Stark, M. S. *J. Am. Chem. Soc.* **2000**, *122*, 4162.

(20) Chen, C.-J.; Bozzelli, J. W. *J. Phys. Chem. A* **2000**, *104*, 4997.

(21) Rienstra-Kiracofe, J. C.; Allen, W. D.; Schaefer, H. F., III. *J. Phys. Chem. A* **2000**, *104*, 9823.

(22) Miller, J. A.; Klippenstein, S. J.; Robertson, S. H. *Proc. Combust. Inst*. **2000**, *28*, 1479.

(23) Miller, J. A.; Klippenstein, S. J. *Int. J. Chem. Kinet.* **2001**, *33*, 654.

(24) Bozzelli, J. W.; Sheng, C. *J. Phys. Chem. A* **2002**, *106*, 1113.

(25) Sheng, C. Y.; Bozzelli, J. W.; Dean, A. M.; Chang, A. Y. *J. Phys. Chem. A* **2002**, *106*, 7276.

(26) Ruiz, R. P.; Bayes, K. D. *J. Phys. Chem.* **1984**, *88*, 2592−2595.

(27) Slagle, I. R.; Park, J.; Gutman, D. *Twentieth Symposium (International) on Combustion*; The Combustion Institute: Pittsburgh, PA, 1984; pp 733−741.

(28) Kaiser, E. W.; Wallington, T. J. *J. Phys. Chem.* **1996**, *100*, 18770−18774.

(29) DeSain, J. D.; Clifford, E. P.; Taatjes, C. A. *J. Phys. Chem. A* **2001**, *105*, 3205−3213.

(30) (a) DeSain, J. D.; Klippenstein, S. J.; Miller, J. A.; Taatjes, C. A. *J. Phys. Chem. A* **2003**, *107*, 4415−4427. (b) DeSain, J. D.; Klippenstein, S. J.; Miller, J. A.; Taatjes, C. A. *J. Phys. Chem. A* **2004**, *108*, 7127−7128.

(31) DeSain, J. D.; Taatjes, C. A.; Miller, J. A.; Klippenstein, S. J.; Hahn, D. K. *Faraday Discuss.* **2001**, *119*, 101−120.

(32) Naik, C.; Carstensen, H.-H.; Dean, A. M. Proceedings of the Third Joint Meeting of the U.S. Sections of the Combustion Institute, Chicago, IL, 2003.

(33) Chan, C.-J.; Hamilton, I. P.; Pritchard, H. O. *Faraday Trans.* **1998**, *94*, 2303−2306.

(34) Chan, C.-J.; Hamilton, I. P.; Pritchard, H. O. *Phys. Chem. Chem. Phys.* **1999**, *1*, 3715−3719.

(35) Zalyubovsky, S. J.; Glover, B. G.; Miller, T. A.; Hayes, C. J.; Merle, J. K.; Hadad, C. M. *J. Phys. Chem. A* **2005**, *109*, 1308−1315.

(36) Frisch, M. J.; Trucks, G. W.; Schlegel, H. B.; Scuseria, G. E.; Robb, M. A.; Cheeseman, J. R.; Montgomery, J. A., Jr.; Vreven, T.; Kudin, K. N.; Burant, J. C.; Millam, J. M.; Iyengar, S. S.; Tomasi, J.; Barone, V.; Mennucci, B.; Cossi, M.; Scalmani, G.; Rega, N.; Pettersson, G. A.; Nakatsuji, H.; Hada, M.; Ehara, M.; Toyota, K.; Fukuda, R.; Hasegawa, J.; Ishida, M.; Nakajima, T.; Honda, Y.; Kitao, O.; Nakai, H.; Klene, M.; Li, X.; Knox, J. E.; Hratchian, H. P.; Cross, J. B.; Adamo, C.; Jaramillo, J.; Gomperts, R.; Stratmann, R. E.; Yazyev, O.; Austin, A. J.; Cammi, R.; Pomelli, C.; Ochterski, J. W.; Ayala, P. Y.; Morokuma, K.; Voth, g. A.; Salvador, P.; Dannenberg, J. J.; Zakrzewski, V. G.; Dapprich, S.; Daniels, A. D.; Strain, M. C.; Farkas, O.; Malick, D. K.; Rabuck, A. D.; Raghavachari, K.; Foresman, J. B.; Ortiz, J. V.; Cui, Q.; Baboul, A. G.; Clifford, S.; Cioslowski, J.; Stefanov, B. B.; Lui, G.; Liashenko, A.; Piskorz, P.; Komaromi, I.; Martin, R. L.; Fox, D. J.; Keith, T.; Al-Laham, M. A.; Peng, C. Y.; Nanayakkara, A.; Challacombe, M.; Gill, P. M. W.; Johnson, B.; Chen, W.; Wong, M. W.; Gonzalez, C.; Pople, J. A. *Gaussian 03*, revision B.04; Gaussian, Inc.; Pittsburgh, PA, 2003.

(37) Becke, A. D. *J. Chem. Phys.* **1993**, *98*, 5648.

(38) Lee, C.; Yang, W.; Parr, R. G. *Phys. Rev. B* **1998**, *37*, 785−789.

(39) Lynch, B. J.; Fast, P. L.; Harris, M.; Truhlar, D. G. *J. Phys. Chem. A* **2000**, *104*, 4811.

(40) Montgomery, J. A., Jr.; Frisch, M. J.; Ochterski, J. W.; Petersson, G. A. *J. Chem. Phys.* **1999**, *110*, 2822−2827.

(41) (a) Gonzalez, C.; Schlegel, H. B. *J. Chem. Phys.* **1989**, *90*, 2154. (b) Gonzalez, C.; Schlegel, H. B. *J. Phys. Chem.* **1990**, *94*, 5523.

(42) Scott, A. P.; Radom, L. *J. Phys. Chem.* **1996**, *100*, 16502−16513.

(43) Lynch, B. J.; Truhlar, D. G. *J. Phys. Chem. A* **2001**, *105*, 2936−2941.

(44) Knyazev, V. D.; Slagle, I. R. *J. Phys. Chem. A* **1998**, *102*, 1770−1778.

(45) Please note that the collaborating authors use a naming convention utilizing all upper case letters as opposed to alternating upper and lower case letters. Furthermore, in ref 35 the naming order started at the terminal methyl carbon as opposed to the terminal peroxy oxygen.

(46) Zalybovsky, S. J.; Tarczay, G.; Miller, T. A. *Chem. Phys. Lett*., submitted.

(47) Viskolcz, B.; Lendvay, G.; Körtvélyesi, T.; Seres, L. *J. Am. Chem. Soc.* **1996**, *118*, 3006−3009.

(48) Lendvzy, G.; Viskolcz, B. *J. Phys. Chem. A* **1998**, *102*, 10777−10786.

(49) The $\langle S^2 \rangle$ values for the Hartree−Fock wave functions are ∼0.91, ∼0.82, and ∼0.80 for the ab initio components for the transition state structures TS(1,4_{elim}), TS(1,4), and TS(1,5), respectively.

(50) Green, W. H.; Wijaya, C. D.; Yelvington, P. E.; Sumathi, R. *Mol. Phys.* **2004**, *102*, 371−380.

(51) The calculations were performed using software provided via personal communication by Dr. Timothy A. Barckholtz, ExxonMobil Research and Engineering Company, Annandale, NJ.